

DiffAxE: Diffusion-driven Hardware Accelerator Generation and Design Space Exploration

Arkapravo Ghosh, *Graduate Student Member, IEEE*, Abhishek Moitra, *Graduate Student Member, IEEE*, Abhiroop Bhattacharjee, *Graduate Student Member, IEEE*, Ruokai Yin, *Graduate Student Member, IEEE*, Priyadarshini Panda, *Member, IEEE*

Abstract—Design space exploration (DSE) is critical for developing optimized hardware architectures, especially for AI workloads such as deep neural networks (DNNs) and large language models (LLMs), which require specialized acceleration. As model complexity grows, accelerator design spaces have expanded to $O(10^{17})$, becoming highly irregular, non-convex, and exhibiting many-to-one mappings from design configurations to performance metrics. This complexity renders direct inverse derivation infeasible and necessitates heuristic or sampling-based optimization. Conventional methods—including Bayesian optimization, gradient descent, reinforcement learning, and genetic algorithms—depend on iterative sampling, resulting in long runtimes and sensitivity to initialization. Deep learning-based approaches have reframed DSE as classification using recommendation models, but remain limited to small-scale ($O(10^3)$), less complex design spaces. To overcome these constraints, we propose a generative approach that models hardware design as 1-D image synthesis conditioned on target performance, enabling efficient learning of non-differentiable, non-bijective hardware-performance mappings. Our framework achieves 0.86% lower generation error than Bayesian optimization with a $17,000\times$ speedup, and outperforms GANDSE with 30% lower error at only $1.83\times$ slower search. We further extend the method to a structured DSE setting, attaining 9.8% lower energy-delay product (EDP) and 6% higher performance, with up to $145.6\times$ and $1312\times$ faster search compared to existing optimization methods on $O(10^{17})$ design spaces. For LLM inference, our method achieves $3.37\times$ and $7.75\times$ lower EDP on a 32nm ASIC and Xilinx Ultrascale+ VPU13 FPGA, respectively, compared to the state-of-the-art DOSA framework.

Index Terms—Denosing diffusion probabilistic model, design automation, design space exploration, DNN accelerator, latent space representation.

I. INTRODUCTION

THE rapid advancement of AI applications has led to an unprecedented demand for specialized hardware capable of efficiently accelerating deep neural network (DNN) inference. As workloads grow increasingly complex and pervasive, spanning domains from data centers to edge devices, designing application-specific hardware becomes essential to achieve optimal power-performance tradeoffs [1], [2]. This has created an urgent need for fast hardware architecture generation and design space exploration tools that can keep pace with the evolving landscape of AI workloads, while balancing tight constraints on power, performance, and area.

AI accelerators are specialized hardware optimized for DNN inference across platforms, from cloud to IoT [1], [3]. A

TABLE I
ACCELERATOR DESIGN PARAMETERS

Design Parameter	Typical Range
MAC array size (R, C)	4 – 128 (integers only)
Buffer Size (IPsz, WTSz, OPSz)	4–1024 kB (step: 128 B)
DRAM Bandwidth (BW)	2 – 32 B/cycle (step: 1 B/cycle)
Loop Order	mnk, nmk, knm, nkm, mkn, kmn
Total design space	1.5×10^{18}

typical single-core accelerator design (Fig. 1(a)) uses systolic arrays of multiply-and-accumulate (MAC) units with on-chip buffers for streaming data to and from off-chip DRAM. Inference involves tiled matrix multiplications between inputs and weights. In this work, we define an AI workload as a general matrix multiply (GEMM) operation, which dominates the computation in LLMs and Vision Transformers (ViTs). Performance is primarily measured by runtime and unless stated otherwise, we refer to the inference runtime as the performance. The performance p depends both on the hardware design HW and the GEMM workload (w). More formally, we can write $p = f(HW, w)$, where f is the mapping between performance and the (hardware, workload) pair. The hardware design can be expressed in terms of the following seven key design parameters—array size, loop order (or dataflow), buffer size, and DRAM bandwidth (refer to Table I). We formally define the accelerator design space \mathcal{D} as the set of all possible unique combinations of these design parameters. In other words, the total design space size $|\mathcal{D}|$ can be expressed as $|\mathcal{D}| = |R| \times |C| \times |IPsz| \times |WTSz| \times |OPsz| \times |BW| \times |LoopOrder|$, where $|\cdot|$ refers to the cardinality or possible design choices for each of the parameters. These hardware parameters have been found to jointly affect the performance of deep learning accelerators (DLAs) such as Eyeriss [4] and Simba [5], forming a vast hardware design space of $O(10^{13-17})$ [6].

Fig. 2 illustrates two critical aspects of the performance landscape for accelerator microarchitecture. First, the inference runtime for a given AI workload is a many-to-one function of the hardware parameters. Fig. 2(a) demonstrates this behavior for the QKV layer of the DeiT-B model [7] across 7.7×10^4 design points, which represent a subset of the design space described in Table I. Secondly, the runtime is a non-differentiable, non-convex and highly discontinuous function of the hardware parameters. As shown in Fig. 2(b), the principal component analysis (PCA) of the runtime across the 7.7×10^4 design points for DeiT-B QKV layer repre-

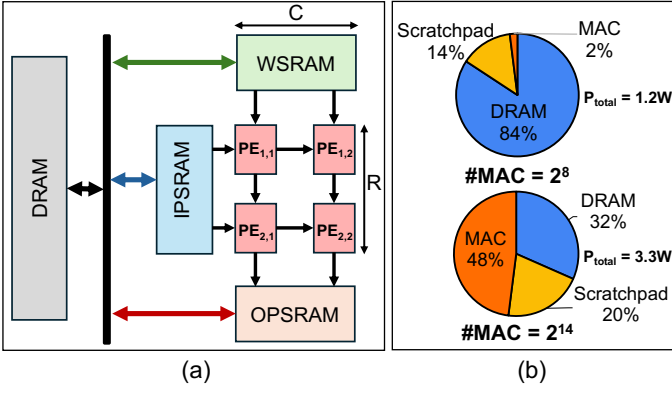


Fig. 1. (a) An $R \times C$ systolic-array based AI accelerator architecture: $PE_{i,j}$ denotes the MAC unit at row i , column j . IPSRAM, WSRAM, and OPSRAM are on-chip buffers for inputs, weights, and outputs, respectively. These buffers interface with off-chip DRAM over a link with bandwidth BW bytes/cycle. (b) Component-wise power consumption of an AI accelerator at 32nm technology: DRAM dominates at low compute densities, whereas compute units become the primary contributors at higher compute intensities.

sents significant irregularities in the performance function that maps the microarchitecture to the inference runtime. While the first challenge implies the non-existence of an inverse function to directly obtain an accelerator design achieving a target performance, the second further precludes solutions based on differential approximation [8] and gradient-descent techniques [8]–[10]. This underscores the necessity for rapid, performance-driven hardware generation and DSE methodologies for accelerators, aimed at minimizing time-to-deployment.

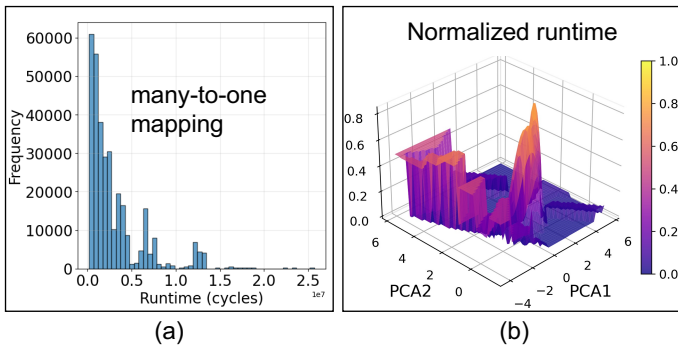


Fig. 2. (a) Many-to-one mapping of hardware configuration to runtime: different hardware designs achieve the same runtime for executing the QKV layer of DeiT-B model (decode stage). (b) Irregular and non-convex nature of the hardware to runtime mapping function for the DeiT-B QKV layer (decode stage).

Current state-of-the-art DSE methods for accelerator design can be broadly categorized into: (1) heuristic-based approaches, (2) black-box optimization, (3) deep learning (DL)-based recommendation models, and (4) generative AI for electronic design automation (EDA). Heuristic methods leverage performance simulators such as TimeLoop [11], Accelergy [12], and Scale-Sim [13] to exhaustively evaluate design points, but are computationally intensive. Black-box optimization techniques including gradient descent (GD) [6], [8]–[10], reinforcement learning (RL) [14], genetic algorithms

[15]–[17], and Bayesian optimization (BO) [6], [18], [19]—offer reduced search times while maintaining comparable performance, but still require several hours. For instance, GAMMA [15] and ConfuciusX [14] take 6–10 hours for large design spaces, while BO and GD-based methods [8], [19] report 3–6 hour runtimes for spaces of size $\sim O(10^7)$. Additionally, their efficiency is sensitive to sampling strategies and initialization [20].

DL-based methods such as AIRCHITECT [21] and AIRCHITECT-v2 [20] train a recommendation model to predict the most optimal accelerator design for a target AI workload. AIRCHITECT employs a classification-based approach to predict the optimal design across a design space of 768 points. However, this method does not scale to larger design spaces, as the number of neurons in the output layer of the recommendation model grows prohibitively large, making it impractical. AIRCHITECT-v2 solves this partially by allowing a classification+regression policy. Although these methods have demonstrated good generalization across a diverse set of AI workloads, they operate on an extremely small (fewer than $O(10^3)$) and simple design space consisting of only two design parameters: the number of MAC units and the total buffer size. Furthermore, these methods are limited to predicting only the optimal design, rather than generating performance-conditioned accelerator designs, thereby restricting their functionality.

While AI for EDA tools have shown promise in tasks such as High-Level Synthesis (HLS) for accelerators—evident in systems like BlockLove [22] and GPT4AIGChip [23]—and in emerging areas like in-memory computing [24], quantum circuits [25], and VLSI design specification [26], these methods primarily operate at higher abstraction levels. They often rely on predicting PPA metrics from RTL specifications [27]–[30], without engaging in fine-grained microarchitecture-level optimization. Although GPT4AIGChip [23] generates HLS code snippets tailored to user-defined latency and energy goals, it relies on a tournament selection-based evolutionary algorithm [31] for obtaining the optimal design parameters. While effective in some cases, this approach can be sample-inefficient and time-consuming. This highlights a critical gap: the lack of AI-driven tools that can assist in design space exploration and optimization at the architectural level for DNN accelerators. Addressing this gap is essential to enable rapid and effective co-design of AI models and their underlying hardware.

In contrast to conventional methods, GANDSE [32], a generative adversarial network (GAN)-based approach, can produce accelerator designs for a given target performance within milliseconds—highlighting the potential of generative models to dramatically reduce search time in design space exploration. GANDSE trains its generator by minimizing the difference between the generated design’s performance and the user-specified target, using a surrogate differentiable function to approximate the true performance landscape. Although GANDSE is trained using gradient descent (GD), it bypasses GD during inference by directly generating hardware designs for a target performance. It leverages CUDA parallelism on GPU to produce diverse configurations within milliseconds,

eliminating the need for time-consuming, sample-dependent optimization. However, this approximation introduces significant error, with an average performance gap of 35% across various AI workloads. Additionally, GANDSE is limited to a relatively small design space (around $O(10^6)$) and targets a narrow set of convolutional neural network (CNN) workloads, which lack diversity in key architectural parameters such as stride, channel sizes, and kernel dimensions [33]. While generative models show promise due to their speed, there remains a gap in applying them to generate hardware accurately for diverse workloads and larger design spaces.

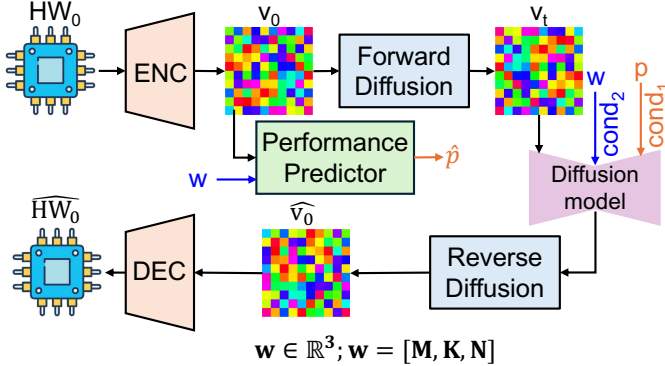


Fig. 3. Overview of DiffAxE: Hardware configurations (HW_0) are encoded into a latent space (v_0) using an autoencoder with a performance-aware latent structure. A diffusion model is trained on these vectors, conditioned on hardware performance (p) and workload (w). w refers to the activation (M , K) and weight (K , N) dimensions. At inference, hardware is generated in latent space based on target p and w , then decoded back to the original space via the autoencoder’s decoder.

To this end, we propose DiffAxE, a diffusion-based generative framework that overcomes the limitations of prior approaches, including slow and sampling-dependent search [6], [14], [15], [19], constrained and less comprehensive design spaces [20], [21], and substantial errors between the target and generated performance [32].

Key idea: Train a conditional diffusion model on a coarse-grained, smaller subset of the target design space to learn the mapping between performance and the hardware. The trained model is then used to generate newer configurations in the targeted design space meeting the target performance which is passed as the condition.

As illustrated in Fig. 3, DiffAxE begins by encoding hardware configurations into a performance-aware latent space using a performance predictor (PP) and an autoencoder (AE), which is an encoder (ENC)-decoder (DEC) network. Subsequently, a conditional denoising diffusion model (DDM) is trained on this latent space, conditioned on two factors: the performance of the hardware configuration (p , denoted as $cond_1$ in Fig. 3) and the workload (w , denoted as $cond_2$) for which the hardware design achieves the performance p . In this context, the workload can be fully described in terms of the GEMM dimensions (M , K , N), where (M , K) is the activation shape and (K , N) is the weight shape. After training, the DDM is employed to generate latent representations of hardware designs that satisfy user-specified performance constraints

for a given workload, which are subsequently decoded into complete hardware configurations via the DEC module. By modeling the conditional distribution in latent space, DiffAxE supports diverse configurations for the same target, addressing the non-invertibility of performance mappings (Fig. 2(a)) and smoothening the design space for stable DDM training (Fig. 2(b)). Our contributions are summarized as:

- 1) **DiffAxE** first leverages a diffusion model for performance-conditioned microarchitecture design automation in AI accelerators. By learning a surrogate inverse of the many-to-one performance function, it enables direct generation of hardware configurations meeting target performance within $\pm 5.45\%$ tolerance in a design space of $O(10^{17})$ at **1.83 milliseconds** per configuration—a **17322 \times** speedup over black-box optimization methods.
- 2) DiffAxE is validated on **600 DNN workloads** (vs. ~ 70 in prior works like VAESA [6], Polaris [19] and DOSA [8]). Trained on $O(10^4)$ samples per workload, it explores design spaces of size $O(10^{17})$ using a lightweight **3.4 million** parameter diffusion model trained in **7 hours** on a single **NVIDIA V100 GPU**.
- 3) DiffAxE, when extended to a structured DSE, achieves **9.8%** average EDP reduction compared to VAESA [6] with **145.6 \times** faster search (**16.5 seconds**). For LLM inference, it delivers up to **4.3 \times** and **5.6 \times** lower EDP than NVDLA [34] and DOSA [8] designs, respectively.
- 4) When conditioned to generate extremely low EDP designs, DiffAxE discovers designs with up to **16%**, **10%** and **14%** higher performance than AIRCHITECT v2 [20], VAESA [6] and the training data respectively, using **32% fewer** parameters than AIRCHITECT v2 [20] and **1312 \times** faster search than VAESA [6].

II. BACKGROUND OF DIFFUSION MODELS

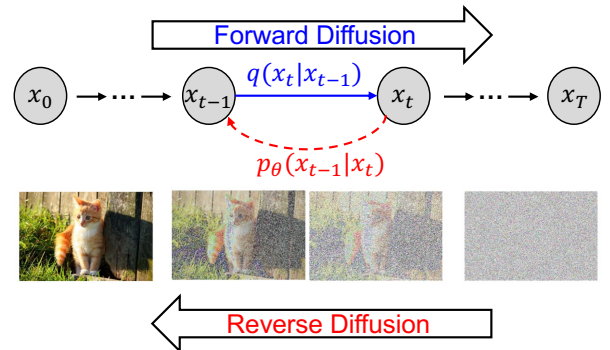


Fig. 4. Basic mechanism of denoising diffusion models (DDMs): forward diffusion iteratively adds noise to the original image, while reverse diffusion involves conditional iterative denoising to generate an image from a Gaussian noise.

Diffusion models are generative models that learn complex data distributions via a two-stage process: a forward pass that gradually adds noise, and a reverse pass that denoises to reconstruct realistic samples as shown in Fig. 4. Unlike GANs, they offer stable training and effectively capture multimodal

outputs, achieving state-of-the-art results in image [35], audio [36], and structured data generation. The diffusion model can be described with the following processes:

Forward Diffusion: The forward diffusion process gradually perturbs a data sample $\mathbf{x}_0 \sim p_{\text{data}}(\mathbf{x})$ over T time steps by adding Gaussian noise. This produces a sequence of latent variables $\mathbf{x}_1, \mathbf{x}_2, \dots, \mathbf{x}_T$, where each \mathbf{x}_t is sampled as:

$$\mathbf{x}_t = \sqrt{\bar{\alpha}_t} \mathbf{x}_0 + \sqrt{1 - \bar{\alpha}_t} \epsilon, \quad \epsilon \sim \mathcal{N}(\mathbf{0}, \mathbf{I}). \quad (1)$$

with $\bar{\alpha}_t = \prod_{s=1}^t \alpha_s$ and $\alpha_t = 1 - \beta_t$, where $\{\beta_t\}_{t=1}^T$ is a predefined noise schedule.

Training Objective: As proposed in [37], the training loss is simplified to a denoising score matching objective. The model is trained to predict the added noise ϵ using the following objective:

$$\mathcal{L}_{\text{simple}} = \|\epsilon - \epsilon_{\theta}(\mathbf{x}_t, t)\|^2 \quad (2)$$

where, ϵ_{θ} is the predicted noise.

Reverse Diffusion: The reverse diffusion process aims to iteratively denoise a sample over T steps to recover data from Gaussian noise. Since the true reverse conditional $q(\mathbf{x}_{t-1}|\mathbf{x}_t)$ is intractable, it is approximated by a parameterized Gaussian distribution:

$$p_{\theta}(\mathbf{x}_{t-1}|\mathbf{x}_t) = \mathcal{N}(\mathbf{x}_{t-1}; \boldsymbol{\mu}_{\theta}(\mathbf{x}_t, t), \boldsymbol{\Sigma}_{\theta}(\mathbf{x}_t, t)). \quad (3)$$

The variance $\boldsymbol{\Sigma}_{\theta}$ is typically fixed as $\sigma_t^2 = \beta_t$. In practice, the model is trained to predict the noise $\epsilon_{\theta}(\mathbf{x}_t, t)$ added during the forward process, from which the mean is computed as:

$$\boldsymbol{\mu}_{\theta}(\mathbf{x}_t, t) = \frac{1}{\sqrt{\alpha_t}} \left(\mathbf{x}_t - \frac{1 - \alpha_t}{\sqrt{1 - \alpha_t}} \epsilon_{\theta}(\mathbf{x}_t, t) \right). \quad (4)$$

At inference time, sampling begins from noise $\mathbf{x}_T \sim \mathcal{N}(\mathbf{0}, \mathbf{I})$ and proceeds via:

$$\mathbf{x}_{t-1} = \boldsymbol{\mu}_{\theta}(\mathbf{x}_t, t) + \sigma_t \mathbf{z}, \quad \mathbf{z} \sim \begin{cases} \mathcal{N}(\mathbf{0}, \mathbf{I}) & \text{if } t > 1, \\ \mathbf{0} & \text{if } t = 1. \end{cases} \quad (5)$$

This iterative denoising process continues for T steps to yield the final generated sample. Given the demonstrated effectiveness of diffusion models in conditional image generation tasks [35], [37], [38], we employ a denoising diffusion model (DDM) that conditions on the desired performance to generate accelerator designs. Recognizing that an accelerator design encodes the relationships between design parameters as a graph structure, we represent this design as a one-dimensional image sequence, which is then generated by the diffusion process conditioned on the performance criteria.

III. METHODOLOGY

Design rationale: Our goal is to learn the mapping f between hardware-workload pairs and performance using a conditional denoising diffusion model (DDM). The model is trained on hardware designs, conditioned on the workload (w) and corresponding performance (p). Once trained, the DDM receives a random noise input and iteratively denoises it based on these conditioning signals, as described in Eqs.(3)–(5), to generate a hardware design achieving the target performance for the given workload. To facilitate learning of this complex mapping, we employ a performance-guided encoding mechanism

using an autoencoder (AE) and a performance predictor (PP) inspired from [6], [19]. This leads to projecting hardware configurations into a latent space where designs with similar performance exhibit a higher cosine similarity. This structured latent space enhances the DDM’s capacity to model the complex hardware–performance relationship, thereby improving performance-conditioned design generation, analogous to image synthesis through stable diffusion [35]. To enable this, we adopt a two-phase approach as shown in Fig. 5. In Phase 1 (ϕ_1), the AE and PP are jointly trained to construct a performance-aware latent space that can be decoded back to the original hardware design. In Phase 2 (ϕ_2), the DDM is trained on latent hardware vectors (v), learning to predict the injected noise in the perturbed latent v_t , conditioned on the timestep (t), workload (w), and performance (p). Once trained, the DDM generates latent vectors meeting the performance requirements for the target workload, which are decoded to recover the corresponding hardware design parameters (refer to Table I). The detailed methodology is described below.

A. Phase 1: Performance-guided encoding

As shown in Fig.6, we represent the accelerator hardware design as a 7-dimensional vector comprising the design parameters listed in Table I. Among these, all parameters are numerical except loop order, which is categorical. To unify the representation, we embed the loop order into an 8-dimensional continuous vector using a learnable linear embedding (Emb_1), and concatenate it with the remaining numerical features to form a 14-dimensional input vector. This concatenated vector is passed through a 3-layer multi-layer perceptron (MLP) encoder (ENC): $\text{Linear}(14, 512) \rightarrow \text{Linear}(512, 256) \rightarrow \text{Linear}(256, 128)$. A symmetric decoder maps the latent vector v back to \mathbb{R}^{14} , and the embedded loop order segment is further processed by a second embedding layer (Emb_2) to recover the original categorical loop order. All the layer dimensions are chosen heuristically and in power of two, a standard practice in deep learning. If trained with the standard reconstruction loss of $\mathcal{L}_{\text{recon}} = \|HW - \hat{H}\hat{W}\|^2$, this creates a reconstructible latent space representation of the hardware designs.

While the autoencoder (AE) and embedding layers create a reconstructible latent representation of the hardware features, it lacks semantic organization with respect to performance. We introduce a performance predictor (PP) trained jointly with the AE. The PP is trained to predict the hardware performance from the latent vectors, thereby inducing a performance-aware latent space representation. The PP comprises of two branches: (1) a workload processor and (2) a latent performance processor. The workload processor is a 4-layer MLP that maps the 3-dimensional workload vector w to a scalar, with the following architecture: $\text{Linear}(3, 256) \rightarrow \text{Linear}(256, 256) \rightarrow \text{Linear}(256, 128) \rightarrow \text{Linear}(128, 1)$. The performance processor is a linear embedding that projects the latent vector v to a 1D scalar ($n_p = 1$ in Fig. 5). The final predicted performance \hat{p} is obtained by summing the outputs of the two branches. Thus, the PP learns a differential function $g(v, w) \approx f(HW, w)$, trained via the mean squared

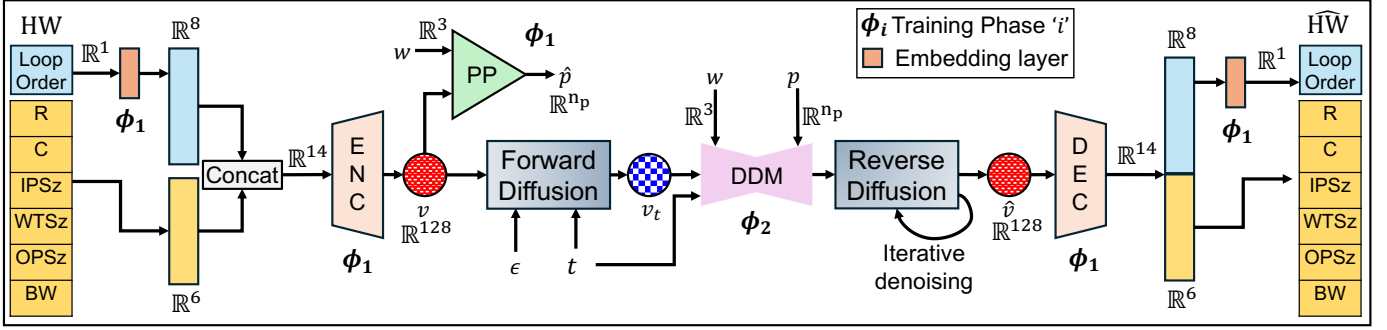


Fig. 5. End-to-end DiffAxE framework: In Phase 1 (ϕ_1), the 7-dimensional hardware configuration (HW) is encoded into a 128-dimensional latent space using an autoencoder (AE) and a performance predictor (PP). Categorical features such as loop order are projected into an 8D continuous space via a learnable embedding. A semantically organized latent space (v), structured by performance, is constructed. In Phase 2 (ϕ_2), noise is injected into v to create a noisy latent v_t and a conditional denoising diffusion model (DDM) is trained to predict this noise, conditioned on hardware performance (p) and workload (w). During generation, the DDM generates a latent vector \hat{v} from random noise, guided by user-specified target (p, w) through iterative denoising via reverse diffusion. Finally, \hat{v} is decoded via the AE's decoder (DEC) to obtain the corresponding hardware configuration \widehat{HW} .

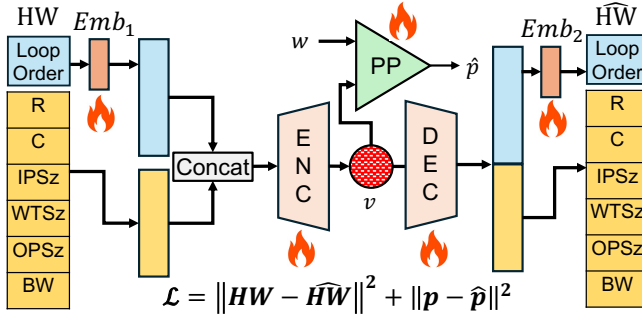


Fig. 6. Phase-1 of DiffAxE: performance-guided encoding of hardware designs into a latent space. The AE ensures reconstruction to the original space while the PP organizes the latent space to encourage lower Euclidean distance between latent vectors with similar performances. 🔥 denotes the trainable modules.

error (MSE) loss: $\mathcal{L}_{\text{pred}} = \|p - \hat{p}\|^2$. The AE, embeddings, and PP are jointly trained to minimize the total loss:

$$\mathcal{L}_{\text{total}} = \mathcal{L}_{\text{recon}} + \mathcal{L}_{\text{pred}}, \quad (6)$$

resulting in a performance-aware latent space. Fig. 7 shows the performance-clustered latent space for a subset of the hardware designs from the design space defined in Table I, for the MLP2 layer of the GPT-2 model [39] during the decode stage. After Phase-1 training, the latent space exhibits a smooth performance gradient varying along two nearly orthogonal directions, with designs clustered coherently according to performance. Although this formulation uses runtime as the performance target, it can be readily extended to multi-dimensional objectives such as [runtime, power], where $n_p > 1$.

B. Phase 2: Diffusion model training

In Phase-2, we train the DDM on the latent space data to predict the noise present in the noisy latent vectors conditioned on the diffusion timestep (t) and the conditioning variables (w and p , as shown in Fig. 8). The DDM consists of two sub-modules, namely the (1) signal processor and the (2) denoising network. The signal processor combines the information from

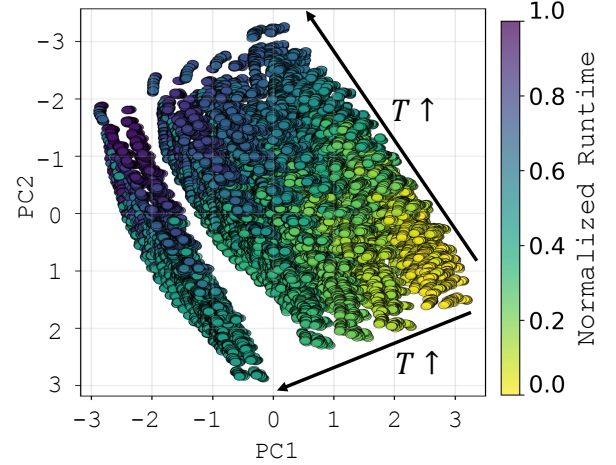


Fig. 7. Latent space (v in Fig. 5(a)) visualization for MLP2 layer of GPT-2 (decode stage) through PCA. PC1 and PC2 refer to the first and the second principal components respectively. Runtime (T) varies continuously along two orthogonal directions, smoothing the highly irregular performance function of Fig. 2(b).

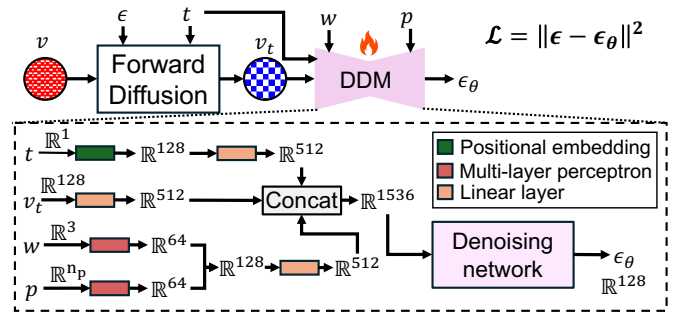


Fig. 8. Phase-2 of DiffAxE: training the DDM conditioned on the workload w and the performance p to predict the noise injected in the noisy latent v_t during forward diffusion. The inset shows how the timestep (t), v_t and the conditioning signals are processed before passing to the denoising network.

the noisy input (v_t), diffusion timestep, and the conditioning variables (w, p) to create a unified representation. This representation is then used as an input to the denoising network

which predicts the amount of noise (ϵ_θ in Fig. 8) in the noisy input. The signal processor consists of the following components:

Time Embedding: We use sinusoidal positional embeddings of dimension 128 to encode the diffusion timestep, which is a 1D scalar quantity. These embeddings are projected to a hidden dimension of 512 via a linear layer.

Condition Embedding: The target performance p and the workload vector $w \in \mathbb{R}^3$ are processed independently via two separate MLPs, each with two linear layers of hidden size 64, ReLU activation, and dropout. The outputs of these condition processors are concatenated and linearly projected to a dimension of 512.

Input Projection: The noisy latent input $v_t \in \mathbb{R}^{128}$ is linearly projected to a hidden dimension of 512 to match the shape of the above mentioned processed signals.

The dimensions of the embedding and the projection layers are chosen heuristically. Next, we describe the denoising network. The denoising network is implemented as an *asymmetric U-Net* that processes a concatenated input vector of size 1536—formed from the projections of the noisy latent vector, the sinusoidal time embedding, and the conditioning signals (performance and workload). The input is processed through a series of downsampling and upsampling blocks interconnected via skip connections. A three-layer MLP downsampling path reduces features from 1536→256 with LayerNorm, ReLU, and dropout, followed by a central 256-dim MLP, then an upsampling path with skip-connected MLPs projecting back to 512 dims. This asymmetric U-Net structure is similar to prior conditional diffusion architectures used in generative modeling [35]. The final hidden vector $\in \mathbb{R}^{512}$ is passed through a linear layer to output the noise prediction $\epsilon_\theta \in \mathbb{R}^{128}$, with the same shape as that of the noisy input v_t .

We use a denoising diffusion probabilistic model (DDPM)-style noise scheduler [37] with a linear β -schedule over $T = 1000$ timesteps. During training, each data point is noised at a randomly sampled timestep, and the model learns to predict this noise via MSE loss, enabling denoising across all diffusion stages.

C. Workload & performance-conditioned hardware generation

After training all modules in DiffAxE, we use the DDM to generate latent hardware configurations conditioned on a target performance and workload. As illustrated in Fig. 9, the generation begins by sampling a noise vector $v_T \sim \mathcal{N}(0, \mathbf{I})$ at the final timestep T . At each step t , the DDM—conditioned on the timestep t , target performance, and workload—predicts the noise to remove and computes the mean $\mu_\theta(v_t, t)$ using the mean computation block (Eq. 4). A small Gaussian noise term $\sigma_t z$ is added to this mean (Eq. 5) to obtain the input for the next timestep $t - 1$. This reverse denoising process continues iteratively until $t = 1$. At the final step, the computed mean is passed to the pretrained decoder (DEC) of the autoencoder from Phase-1, which reconstructs the complete hardware design from its latent representation. Since, we always normalize data before feeding into a neural network, the decoded hardware design is in the normalized domain. Thus, we need to

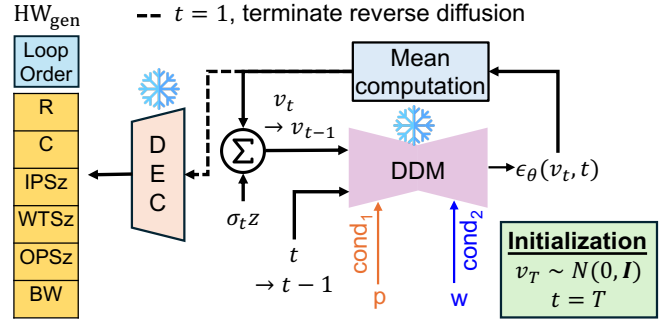


Fig. 9. Conditional hardware generation that achieves a performance p for a workload w . Initially starting with a random noise at timestep T , the DDM predicts the noise ϵ_θ which is fed to the mean computation block (refer to Eq. 4). A small Gaussian perturbation is added to this computed mean (refer to Eq. 5) to obtain the partially denoised input for the next timestep $t = T - 1$. The process repeats iteratively until $t = 1$, when the computed mean is the fully denoised latent hardware design, which is decoded through the DEC of the AE module to obtain the generated hardware design HW_{gen} . * represents frozen modules.

apply inverse transformation to get meaningful values of the design parameters. The inverse transformed design parameters are then rounded off to their nearest allowed state depending on the target design space granularity.

D. DSE for EDP optimization

We extend DiffAxE for performing EDP optimization by exploring the power-performance landscape in the design space. Fig. 10 shows the runtime (performance)-power scatter plot for executing the GEMM operation: $(M, K) \times (K, N)$ with $(M, K, N) = (128, 4096, 8192)$ on a 32nm ASIC implementation across a subset of the design space defined in Table I.

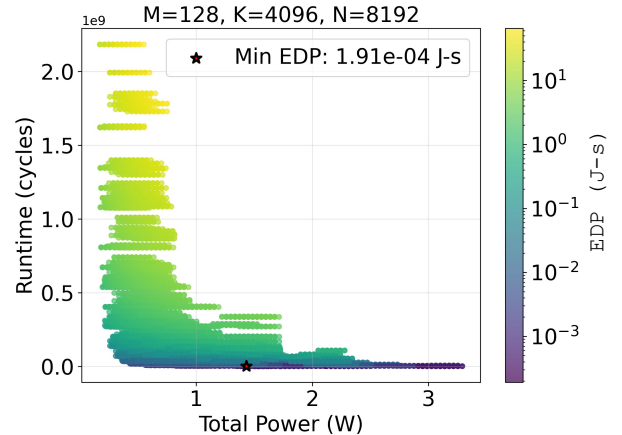


Fig. 10. Performance-power scatter plot for executing the GEMM operation with (M, K, N) as the GEMM dimensions on a 32nm ASIC implementation across 7.7×10^4 hardware designs sampled from the design space defined in Table I.

Different hardware designs can exhibit diverse power and performance characteristics while yielding similar energy-delay product (EDP) values. This motivates conditioning the design space exploration on a variety of (power, performance)

targets, enabling the discovery of novel hardware configurations unseen during training, that achieve lower EDP. To enable this, we modify the performance predictor in Phase-1 to jointly predict power and performance. The loss function is defined as:

$$\mathcal{L}_{PP} = (\text{power} - \hat{\text{power}})^2 + (\text{perf} - \hat{\text{perf}})^2 \quad (7)$$

where, $\hat{\cdot}$ denotes the predicted metric using the PP. This encourages the autoencoder to cluster hardware designs with similar power-performance characteristics in the latent space.

Next, for each workload, we discretize the power and performance metrics into N_{power} and N_{perf} percentile-based bins, respectively. We define the combined class label for each hardware design as:

$$\text{class} = \text{class}_{\text{power}} + N_{\text{power}} \cdot \text{class}_{\text{perf}} \quad (8)$$

where $\text{class}_{\text{power}}$ and $\text{class}_{\text{perf}}$ denote the respective bin indices for power and performance. Fig. 11 shows that joint AE+PP training in Phase-1, using both power and performance supervision, yields a semantically structured latent space organized by power-performance categories. In Phase-

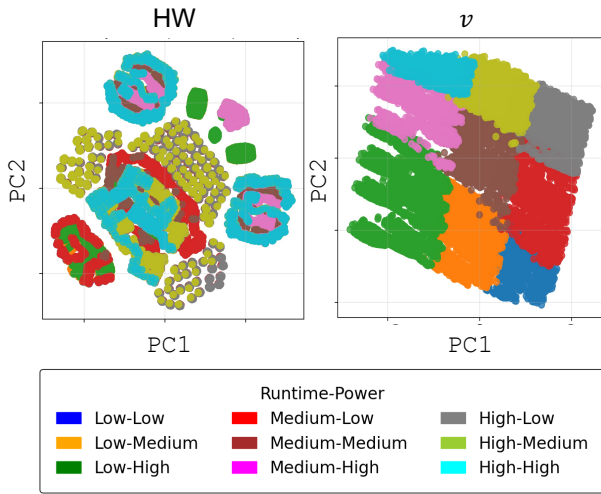


Fig. 11. PCA of latent space (v) from the MLP2 layer (decode stage) in GPT-2 after **Phase-1** training with joint power and performance supervision (Eq. 6). Runtime-power classes are percentile-based (Section IV(D)). While the original hardware space (left) lacks semantic structure, the learned latent space (right) exhibits clear clustering by power-performance characteristics.

2, instead of conditioning the diffusion model on continuous performance values, we condition it on the discrete class label defined in Eq. 8. This enables the diffusion model to learn the mapping between latent hardware representations and their associated power-performance classes. Finally, we generate N_{config} hardware designs for each of the $N_{\text{power}} \times N_{\text{perf}}$ classes and report the lowest EDP discovered.

E. DSE for performance optimization

Fig. 10 shows that lower EDP values are strongly correlated with higher performance (i.e., shorter runtime). This insight motivates the conditional generation of low-EDP designs to discover high-performance configurations using the DiffAxE framework. In Phase-1 of training, we use EDP as the supervision signal, resulting in a latent space that is structured

according to EDP. We then divide the full EDP range into N_{EDP} percentile-based classes for each (M, K, N) workload. These discrete EDP classes serve as the conditioning input during Phase-2 diffusion model training. Once trained, we generate hardware designs conditioned only on class 1 (i.e., the lowest-EDP class) and obtain high-performance designs beyond those seen during training.

IV. EXPERIMENTS

A. Dataset

Each hardware configuration is represented as a 7-dimensional vector comprising the design parameters listed in Table I. We define two key terms to clarify the scope of design generation in DiffAxE: (1) the **training design space**, and (2) the **target design space**. The *training design space* encompasses the set of accelerator configurations used during training to learn the mapping from performance to hardware. In contrast, the *target design space* represents the full set of practically deployable hardware configurations. As shown in Table II, the target design space permits finer-grained choices for systolic array dimensions and buffer sizes, whereas the training design space is a coarser subset that spans the full range of each parameter. The key idea is to train the DiffAxE framework on the coarser training design space ($O(10^4)$), but use the knowledge developed to generalize to even finer design spaces ($O(10^{17})$).

TABLE II
DESIGN PARAMETER RANGES IN TRAINING AND TARGET SPACES:
ALLOWED VALUES OF DESIGN PARAMETERS FOR BOTH THE DESIGN SPACES

Parameter	Training design space	Target design space
R, C	{4, 8, 16, 32, 64, 128}	4–128 (integers)
IPSz, WTSz,	{4, 64, 128, 256, 512, 1024} kB	4–1024 kB (step: 128 bytes)
OPSz	1024} kB	
BW	{2, 4, 8, 16, 32} B/cycle	2–32 B/cycle (step: 1 B/cycle)
Loop Order	mnk, nmk	mnk, nmk
Design space	7.76×10^4	5.26×10^{17}

Next, we define the AI workloads (w) that we consider in this work. We consider **600** distinct workloads with the GEMM dimension ranges as $M : 1\text{--}1024$, $K : 1\text{--}4096$, and $N : 1\text{--}30,000$. The (M, K, N) distribution of the workloads under consideration is shown in Fig. 12. For each workload, we define a coarse-grained training design space of size 7.76×10^4 as described in Table II. In this work, we only consider the two possible loop orders for an output stationary dataflow (OS) [40] as it has been shown to be the most optimal dataflow across a wide variety of GEMM workloads [21]. The performance labels such as runtime, power and EDP are generated for each of the $\{HW, w\}$ tuple to constitute the entire training data of $600 \times (7.76 \times 10^4) = 46.7M$ data points. We use Scale-Sim [13], an open-source cycle-accurate simulator that provides inference runtime for a GEMM operation along with the associated memory access traces at different memory hierarchy. We use CACTI 7 [41] to obtain the DRAM and on-chip buffer energy from the Scale-Sim generated traces for a

32nm process technology. The compute energy is estimated using the MAC energy models defined in NeuroSim [42]. The dataset is made available in the IEEE DataPort repository [DOI: <https://dx.doi.org/10.21227/w2hh-vb37>].

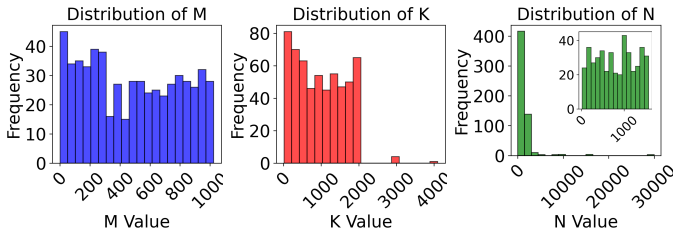


Fig. 12. Workload distribution in the training data. A workload is defined as $w = (M, K, N)$ which denotes the $(M, K) \times (K, N)$ matrix-matrix multiplication.

All numerical features in HW are min-max normalized. The categorical loop order is one-hot encoded and passed through a learnable linear embedding within the encoder (see Fig. 5, Section III). To ensure DiffAxE generalizes across diverse workloads, we address the high runtime variability. As shown in Fig. 13, runtimes can span three orders of magnitude within a single workload and vary significantly across workloads. To mitigate this, we apply a logarithmic transformation followed by workload-wise min-max normalization of runtimes to $[0, 1]$. The workload dimensions (M, K, N) are also min-max normalized. Power values, ranging from 0.17 W to 3.3 W (Fig. 10), are similarly min-max normalized.

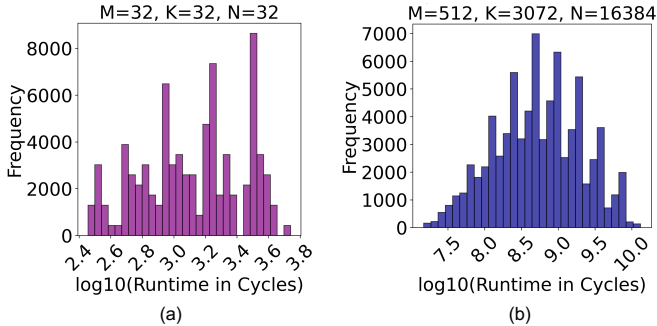


Fig. 13. Runtime distribution of two distinct workloads in the dataset: (a) $(M, K, N)=(32, 32, 32)$ and (b) $(M, K, N)=(512, 3072, 16384)$. Runtimes for each (M, K, N) span over 3 orders of magnitudes, and the range varies across different workloads.

B. Experimental Setup

We evaluate DiffAxE through three key experiments: (1) generating hardware configurations for a target performance p given a workload w , (2) discovering low-EDP designs via power-performance conditioned generation, and (3) generating high-performance designs by conditioning on low-EDP targets. Setup, metrics, and baselines are detailed below.

1) *Performance-specific hardware generation*: In this experiment, we evaluate DiffAxE’s ability to generate hardware designs that match specified target runtimes across 600 workloads. For each workload, we uniformly sample **20** target runtimes between its minimum and maximum observed values,

yielding $600 \times 20 = 12,000$ targets. For each target, **1,000** designs are generated using DiffAxE and evaluated with Scale-Sim [13], resulting in a total of 1.2×10^7 designs. We use the relative generation error as the evaluation metric:

$$error_{gen} = \frac{T_{gen} - T^*}{T^*} \quad (9)$$

where T^* is the target runtime and T_{gen} is the runtime of a generated design. We report the average error across all generated designs. We also adapt two optimization-based baselines—Bayesian Optimization (BO) and Gradient Descent (GD)—by minimizing the following objective:

$$\min(T_{gen} - T^*) \quad (10)$$

We compare DiffAxE against five baselines: vanilla GD (similar to DOSA [8]), vanilla BO, latent-space BO (similar to VAESA [6]), latent-space GD (similar to Polaris [19]), and GANDSE [32]. The vanilla BO and GD baselines operate directly on the hardware design parameters, while the latent-space BO and GD baselines optimize over the continuous and structured latent space obtained after **Phase-1** of DiffAxE (refer to Fig. 6). To ensure robust comparisons, all evaluations are conducted over the full set of 600 workloads. For each workload, we report the average search time and generation error ($error_{gen}$), defined in Eq. (10). To account for stochasticity in initialization, we repeat each experiment using 10 different random seeds. All reported metrics are averaged over these 10 runs. The baselines along with their respective average generation errors and search times are provided in Table III.

TABLE III
COMPARISON OF DIFFAXE WITH BASELINES FOR RUNTIME-SPECIFIC HARDWARE GENERATION

Method	Search Time (s)	$error_{gen}$
Vanilla GD (DOSAs [8])	31.54	31.59%
Vanilla BO	150.19	17.14%
Latent GD (Polaris [19])	30.80	10.08%
Latent BO (VAESA [6])	31.70	6.31%
GANDSE [32]	10^{-3}	34.27%
DiffAxE (ours)	1.83×10^{-3}	5.45%

2) *DSE for EDP optimization*: This experiment evaluates the optimality of designs generated by DiffAxE based on Energy-Delay Product (EDP), where lower EDP indicates higher efficiency. We introduce **Search Performance (SP)** as a metric to compare design space exploration (DSE) strategies, defined as the ratio of EDP from random search to that from a given method as $SP = EDP_{random} / EDP_{DiffAxE}$. Higher SP indicates better design quality. We also report *search time* to measure computational efficiency. We partition power and performance into 3 percentile-based bins each, yielding 9 power-performance classes. For each class, we generate **1000** designs using DiffAxE, totaling 9000 designs per workload. These are evaluated for EDP using Scale-Sim [13] and CACTI 7 [41]. We compare against five baselines: random search, vanilla BO, VAESA [6] (latent BO), DOSA [8] (vanilla GD), and Polaris [19] (latent GD). For fair

comparison, 9000 designs are randomly sampled from the full design space ($O(10^{17})$) for the random baseline. Minimum EDPs per workload are used to compute SP, averaged over all workloads and 10 random seeds to mitigate effects of stochasticity. Table IV summarizes the results.

TABLE IV
COMPARISON OF DIFFAXE WITH BASELINES FOR EDP-ORIENTED DSE.
SP: RELATIVE SEARCH PERFORMANCE NORMALIZED TO RANDOM SEARCH (\uparrow BETTER).

Baseline	Design Space	SP (\uparrow)	Search Time (\downarrow)
Random Search	$O(10^{17})$	1.00	3 milliseconds
Vanilla BO	$O(10^{17})$	0.98	2 hours
VAESA [6]	$O(10^{17})$	1.02	40 minutes
DOSA [8]	$\sim O(10^7)$	0.20	18 minutes
Polaris [19]	$\sim O(10^7)$	0.54	10 minutes
DiffAxE (ours)	$O(10^{17})$	1.12	16.5 seconds

3) *DSE for performance optimization*: We compare the performance of designs generated by DiffAxE against three baselines: AIRCHITECT [21], AIRCHITECT v2 [20], and VAESA [6]. While AIRCHITECT v2 searches over a fixed space of 768 configurations, both VAESA and DiffAxE explore a significantly larger space of $O(10^{17})$ designs. We set $N_{\text{EDP}} = 10$ (see Section III(E)) and generate designs using DiffAxE exclusively from class 1 (top 10% lowest EDP). From this set, we select the highest-performing design and use it to normalize the performance of all baselines. Reported values are averaged over all workloads (Section IV(A)) and over 10 random seeds to reduce stochasticity.

V. RESULTS & ANALYSIS

A. Performance-specific hardware generation

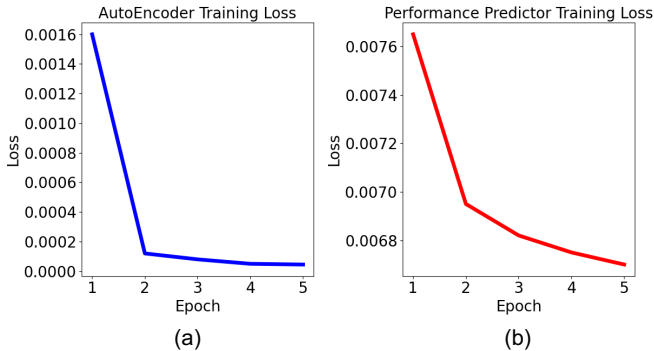


Fig. 14. Training loss curves for Phase-1 training of DiffAxE: (a) Autoencoder loss representing quality of reconstruction (b) Performance predictor loss representing performance prediction capability.

Fig. 14 shows the training curves for AE and PP during **Phase-1** training of DiffAxE. The objective is to map the hardware designs into a latent space organized according to their performance. We train the AE and PP in tandem for 5 epochs, with an initial learning rate of 0.0001, AdamW optimizer [43] with a weight decay of 0.001, and a ReduceLRonPlateau learning rate scheduler with a patience of 2 epochs. We use an NVIDIA V100 GPU for training and generation. We select

a batch size of 512, which does not lead to CUDA out-of-memory (OOM) errors due to the low-dimensional nature of the data (7D compared to a standard $224 \times 224 \times 3$ ImageNet sample [44]).

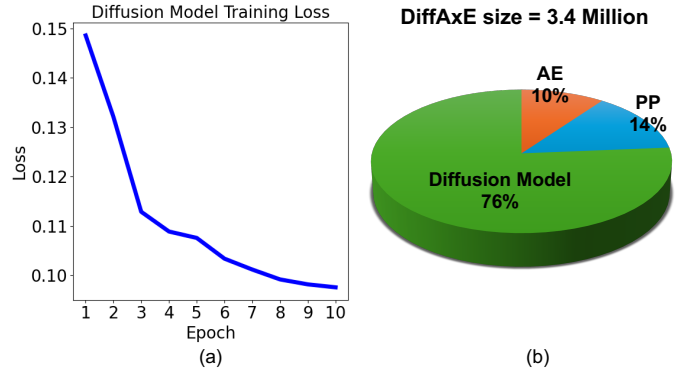


Fig. 15. (a) Training loss curves for Phase-2 training of diffusion model (b) Model size of DiffAxE and component-wise breakdown.

Fig. 15(a) shows the training loss curves for the diffusion model, when trained on the latent space data during **Phase-2**. We train the diffusion model for 10 epochs with an initial learning rate of 0.0001 with an AdamW optimizer having weight decay as 0.01 and a ReduceLRonPlateau learning rate scheduler with a patience of 2 epochs. We select a batch size of 128. Also, DiffAxE is a lightweight model consisting of only 3.4 million trainable parameters as shown in Fig. 15. Further, the training cost is also low as it requires < 7 hours to train with $46.7M$ training data samples on a single NVIDIA V100 GPU.

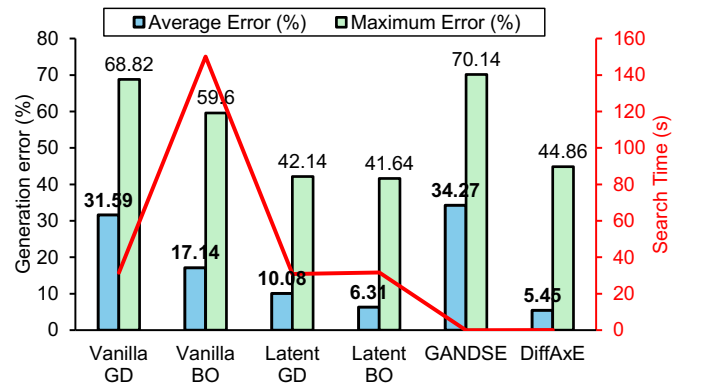


Fig. 16. Comparison of $error_{gen}$ (lower is better) and search time (lower is better) of DiffAxE with baselines defined in Section V(B)-I.

Fig.16 compares DiffAxE against the baselines defined in TableIII. The vanilla gradient descent (GD) approach exhibits a high average generation error ($error_{gen} > 30\%$), indicating that the differential approximation of the performance function f is insufficiently accurate. Since Bayesian optimization (BO) operates as a black-box optimizer, applying BO directly in the hardware space reduces the average generation error by 13% compared to vanilla GD, but at the cost of around 150 seconds of larger search time.

In contrast, latent space methods—both GD and BO—significantly outperform their vanilla counterparts, achieving average generation errors within $\pm 10\%$ in under 30 seconds. This shows the efficacy of applying optimization in the performance-guided latent space, and is in accordance with VAESA and Polaris. GANDSE [32] offers substantial speedup over vanilla GD (approximately $32000\times$), but its generation quality remains comparable. This is because GANDSE, like vanilla GD, relies on the assumption of differentiability in the performance model, resulting in a similar $error_{gen}$. Nevertheless, GANDSE benefits from its GAN-based generator, which enables one-shot design generation without iterative optimization, thus achieving significant runtime gains. DiffAxE not only achieves lower average generation error than the best-performing baseline (latent BO), but also does so with an average generation time of just 1.83 milliseconds—yielding over $17000\times$ speedup compared to latent BO. This proves that employing a diffusion model to learn the hardware to performance mapping in the latent space leads to generation of more accurate performance-aware hardware designs over the traditional optimization techniques of GD and BO.

B. DSE for EDP optimization

As presented in Table IV, DiffAxE achieves a search performance (SP) that is 9.8% higher than VAESA [6], the most competitive baseline employing latent space Bayesian Optimization (BO) within a design space of comparable size and complexity ($O(10^{17})$). Importantly, DiffAxE attains this superior SP within a fixed search time of only 16.5 seconds using $N_{power} = N_{perf} = 3$ classes, resulting in a $145.6\times$ improvement in search speed. In contrast, DOSA [8] and Polaris [19], which rely on vanilla and latent space gradient descent (GD) respectively, yield significantly suboptimal designs—exhibiting lower SP (i.e., higher EDP) than even random search. This underperformance is primarily attributed to their application over a much coarser design space granularity (approximately $O(10^7)$), which limits their optimization effectiveness.

C. DSE for performance optimization

Fig. 17 presents a comparison of the runtimes of designs generated by the baseline methods and those produced by DiffAxE. When compared to VAESA, which employs latent-space BO within the same design space, DiffAxE achieves a 10% improvement in performance while reducing search time by a factor of $1312\times$. Relative to the

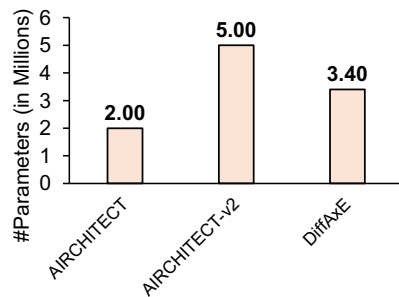


Fig. 18. Comparison of model size (lower is better) between prior DL-based DSE works and DiffAxE.

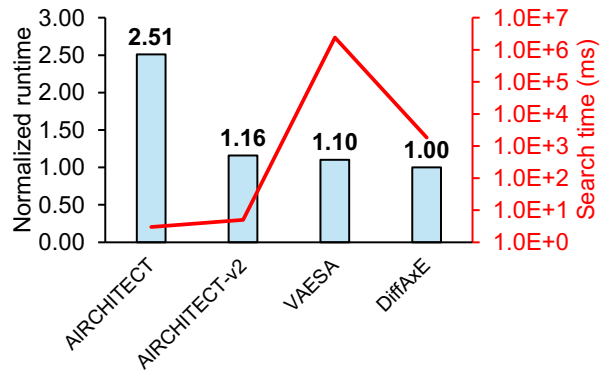


Fig. 17. Normalized runtime (lower is better) and GPU search time (lower is better) of baselines (AIRCHITECT [21], AIRCHITECT-v2 [20] and VAESA [6]) compared to DiffAxE.

DL-based classification approach used in AIRCHITECT, DiffAxE delivers an average performance gain of $2.51\times$. Furthermore, in comparison to AIRCHITECT v2 [20], DiffAxE achieves a 16% improvement in performance. Further, DiffAxE requires 32% lower parameters (and thus, training cost) compared to AIRCHITECT v2 as shown in Fig.18. We now analyze the hardware designs generated by DiffAxE in greater detail.

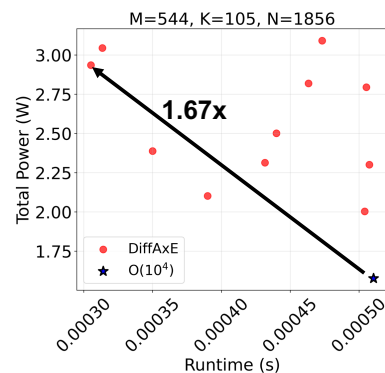


Fig. 19. Power vs. runtime scatter plot of DiffAxE-generated configurations that outperform the training dataset ($O(10^4)$) for $(M, K, N) = (544, 105, 1856)$, showing a $1.67\times$ speedup.

Fig. 19 shows a power-runtime scatter plot of configurations produced by DiffAxE for a given workload, conditioned on class 1 of the EDP metric. The comparison is made against the highest-performing configuration (i.e., lowest runtime) in a training dataset of size $O(10^4)$. Configurations identified by DiffAxE that surpass this baseline are highlighted in red. Table V compares the fastest DiffAxE-

generated designs with the best training-set configurations for each workload. DiffAxE consistently allocates $4\times$ more compute resources and significantly larger input and weight buffers. Using an mnk loop ordering, it emphasizes increasing the weight buffer size (WTSz), enabling the entire weight tensor to remain on-chip. This eliminates the need to re-fetch weight tiles from DRAM—normally incurred by a factor of $\lceil \frac{M}{R} \rceil$ —and results in substantial runtime reduction despite identical DRAM bandwidth.

VI. INFERENCE OPTIMIZATION OF LLMs

In this section, we demonstrate how the DiffAxE framework can be extended to minimize the energy-delay product (EDP) during LLM inference. In chiplet-based systems [45]–[48],

TABLE V
HARDWARE COMPARISON OF FASTEST CONFIGURATIONS FROM DIFFAXE
AND TRAINING DATA FOR $(M, K, N) = (544, 105, 1856)$

Parameter	DiffAxE	Training Data
R	121	32
C	128	128
IPSz (kB)	568	208
WTSz (kB)	1024	4
OPSz (kB)	27	4
BW (B/cycle)	32	32
Loop Order	mnk	nmk

different chiplets can be specialized for distinct inference phases—prefill and decode—and dynamically selected at runtime. Prefill benefits from high-throughput chiplets, while decode favors low-latency, memory-efficient designs. This flexibility allows tailored accelerator configurations across stages, improving overall EDP. Our framework can interface with such heterogeneous accelerators, dynamically routing computation to the most appropriate chiplet for each phase, thus achieving better EDP tradeoffs. Fig. 5 illustrates our methodology using a single GEMM operation, $(M, K) \times (K, N)$, as the workload. We begin by explaining how this approach generalizes to deep neural networks (DNNs), which involve sequences of such GEMM operations. Rather than a single workload of the form (M, K, N) , a DNN comprises a sequence of operations: $[(M_1, K_1, N_1), (M_2, K_2, N_2), \dots, (M_l, K_l, N_l)]$ for an l -layered model. To handle this sequence, we replace the original multi-layer perceptron (MLP)-based performance predictor (PP)—designed for individual GEMM workloads—with an attention-based sequence encoder that captures inter-layer dependencies across the l layers.

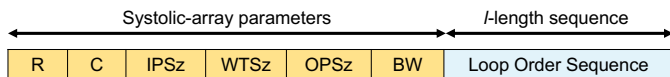


Fig. 20. Data structure of HW in Fig. 5(a) for sequence of l GEMM operations as workload for DNN inference. The loop order sequence represents the independent mapping of each layer in the DNN.

Furthermore, the hardware data representation (denoted as HW in Fig. 5(a)) must support the generation of layer-wise loop orders across the entire DNN, while maintaining fixed systolic array parameters for each layer. Fig. 20 illustrates the structure of the HW data used to represent workloads

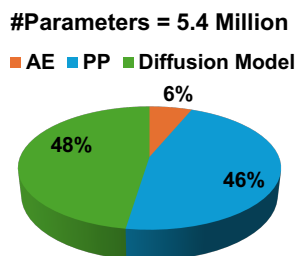


Fig. 21. Model size of DiffAxE for GEMM sequence workloads and component-wise breakdown.

comprising sequences of GEMM operations. The rest of the methodology remains unchanged. While this extension increases the complexity of the PP and results in a larger model size, as shown in Fig. 21, it does not impact generation

time since the diffusion model size and the number of denoising steps (T , see Section II) remain constant. We evaluate the hardware designs generated by DiffAxE for three widely used large language models (LLMs)—LLaMA-2 7B [49], OPT-350M [50], and BERT-base [51]—and compare them against several representative accelerator baselines: Eyeriss [4], NVDLA [34], ShiDianNao [40], and DOSA [8], a differential optimization framework designed to minimize the energy-delay product (EDP) of model inference.

TABLE VI
HARDWARE PARAMETERS OF FIXED DNN ACCELERATOR
ARCHITECTURES

Parameter	Eyeriss [4]	ShiDianNao [40]	NVDLA [34]
PE Array ($R \times C$)	12×14	16×16	32×32
IPSz (kB)	108	32	64
WTSz (kB)	108	32	512
OPSz (kB)	8	8	32
DRAM BW (B/cycle)	16	8	16

Table VI shows the hardware configurations for the three fixed architectures. Fig. 22 presents the EDP of the fixed architecture designs in comparison with designs generated by DOSA and DiffAxE, across both the prefill and decode stages for three representative LLMs. Both DOSA and DiffAxE consistently outperform the fixed architectures, with the performance gap being particularly significant during the prefill stage. This is attributed to the greater flexibility in processing element (PE) array sizing—DOSA and DiffAxE support configurations up to 128×128 , whereas the fixed architectures are constrained to a typical compute capacity of approximately 256–1024 MAC units. For example, compared to NVDLA, DOSA and DiffAxE offer up to a $16 \times$ increase in available compute resources. Also, DOSA and DiffAxE offer up to 32 bytes/cycle of DRAM bandwidth, which is twice as compared to NVDLA. This substantial disparity leads to higher runtimes and consequently elevated energy consumption in the fixed architectures, culminating in a higher EDP. Notably, DiffAxE achieves more than a $2 \times$ reduction in EDP relative to DOSA across all evaluated scenarios. To further understand the architectural advantages, we next examine the designs generated by DOSA and DiffAxE in greater detail. Table VII compares the hardware design and mapping generated by DiffAxE compared to DOSA for the BERT-base model across both prefill and decode stages.

During the prefill stage, DiffAxE predominantly selects the nmk loop ordering. This choice leads to a potential repetition in input activation loads by a factor of $\lceil \frac{N}{C} \rceil$ for the (M, K, N) GEMM operation. To mitigate this, DiffAxE allocates the maximum permissible input buffer size—1 MB in this case—to avoid redundant memory accesses. In contrast, DOSA assigns comparatively smaller buffer sizes to both input and weight operands, resulting in a significantly higher frequency of redundant data fetches. These additional DRAM accesses—limited by relatively low bandwidth—introduce substantial latency, leading to over $2 \times$ longer runtimes for DOSA relative to DiffAxE. Consequently, DOSA incurs nearly a $6 \times$ higher EDP during prefill. In the decode stage, token generation follows an

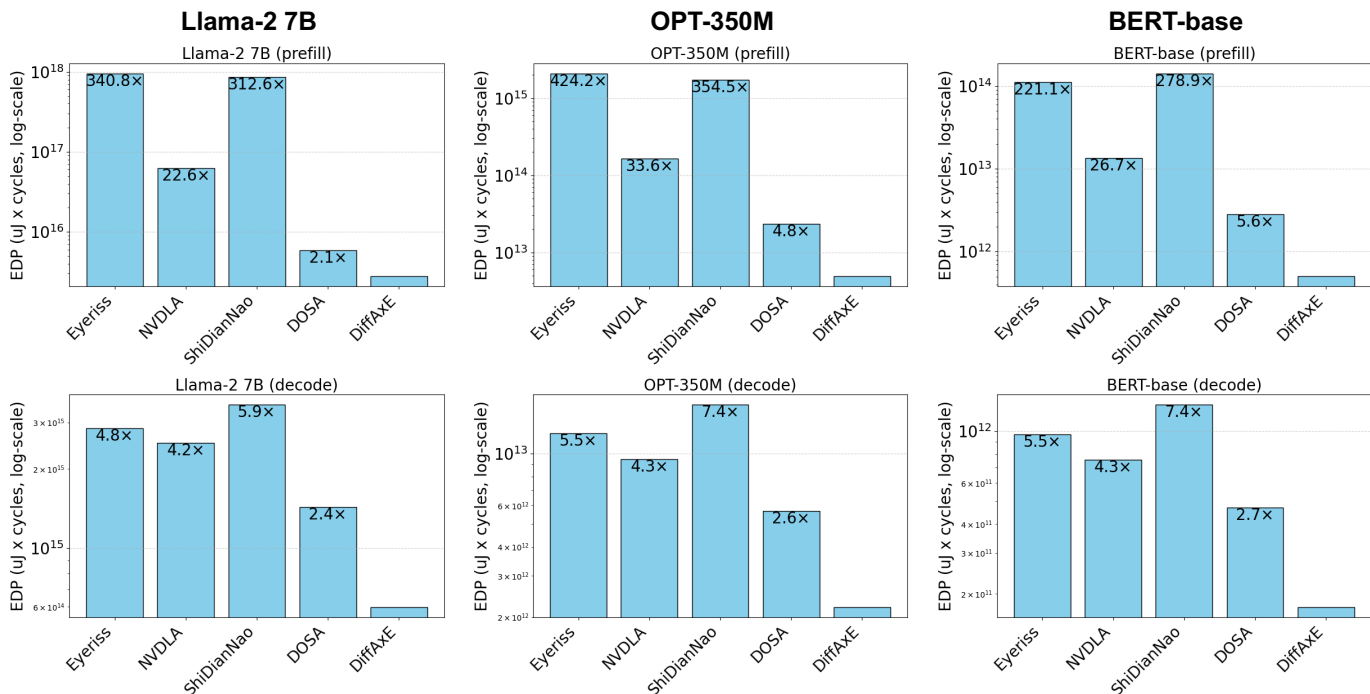


Fig. 22. Energy-delay product (EDP) of baseline accelerators including Eyeriss [4], NVDLA [34], ShiDianNao [40] and DOSA [8]-optimized Gemini, compared to DiffAxE for 32nm ASIC implementation. Prefill represents a default sequence length of 128 tokens. Bar labels represent EDP normalized to DiffAxE.

TABLE VII
HARDWARE DESIGN COMPARISON: DOSA VS. DIFFAXE ON BERT WORKLOADS. LOOP ORDER SHOWN FOR EACH LAYER IN [].

Workload	Method	R	C	IPSz (kB)	WTSz (kB)	OPSz (kB)	BW (B/cycle)	Loop Order [qkv, qk^T , pv, attn_proj, mlp1, mlp2]	Runtime (cycles)	EDP (uJ-cycles)
BERT-Base-prefill	DOSA	128	128	128	128	64	32	[mnk, mnk, mnk, mnk, mnk, mnk]	1.42e+07	2.80e+12
	DiffAxE	128	63	1024	4	8.5	32	[nmk, mnk, mnk, nmk, nmk, nmk]	6.90e+06	5.02e+11
BERT-Base-decode	DOSA	128	128	96	128	32	32	[nmk, mnk, mnk, nmk, nmk, mnk]	5.82e+06	4.71e+11
	DiffAxE	4	64	4	4	8.9	32	[mnk, mnk, mnk, mnk, mnk, nmk]	5.47e+06	1.75e+11

auto-regressive pattern, reducing the matrix row dimension to $M = 1$ across all layers. DiffAxE’s diffusion model identifies this characteristic and accordingly selects a much smaller PE array row count (R), avoiding configurations where $R > M$, which would otherwise lead to severe under-utilization and introduce an additional $(R - M)$ cycle overhead in output-stationary (OS) dataflow due to output draining. Furthermore, DiffAxE predominantly employs the mnk loop ordering across most layers, which, in conjunction with the smaller R values, substantially reduces input buffer requirements. This results in lower dynamic power and reduced SRAM access energy compared to DOSA, which utilizes significantly larger buffers. Although DOSA and DiffAxE achieve comparable runtimes in the decode stage, DOSA suffers from higher on-chip power consumption due to PE under-utilization and inefficient buffer provisioning, resulting in nearly a $3\times$ higher EDP.

FPGA Implementation: Next, we implement the accelerator designs for BERT-base prefill stage on a Xilinx Virtex UltraScale+ VU13P FPGA. The Xilinx Virtex UltraScale+ VU13P is a high-performance 16nm FPGA with 3.78 million logic cells, 12,288 DSP48E2 slices, 455.Mbit on-chip memory, up

to 128 GTY transceivers, and 832 general-purpose I/Os for high-bandwidth interfaces [52], [53]. Each DSP slice supports fixed-point and floating-point operations, making it ideal for compute-intensive DL applications [54]. Fig. 23 shows the

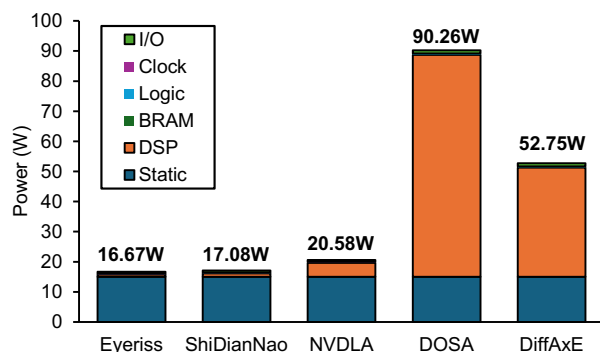


Fig. 23. Power consumption of different architectures on Xilinx Virtex UltraScale+ VU13P FPGA board. The DOSA and DiffAxE designs are for BERT-base prefill stages as in Table VII.

power consumption of various accelerator designs for the

BERT-base prefill stage (see, Table VII). Table VIII shows the component-wise resource utilization for different accelerator designs on this FPGA. For DOSA [8] and DiffAxE, we report utilization for the architectures generated for BERT-Base prefill stage (see Table VII). As expected, DOSA and DiffAxE designs require much larger DSPs due to higher number of MAC units compared to the fixed architectures like NVDLA. Also, DiffAxE consumes highest amount of URAM (UltraRAM) due to largest aggregate on chip buffer size as shown in Table VII.

TABLE VIII
RESOURCE UTILIZATION OF VARIOUS DNN ACCELERATOR ARCHITECTURES

Architectures	#DSP	#LUT	#FF	#BRAM	#URAM
Eyeriss [4]	84	45,696	71,544	10	6
ShiDianNao [40]	128	47,632	74,448	26	0
NVDLA [34]	512	64,528	99,792	31	15
DOSA [8]	8192	360,448	540,672	23	8
DiffAxE	4032	232,408	352,112	11	29

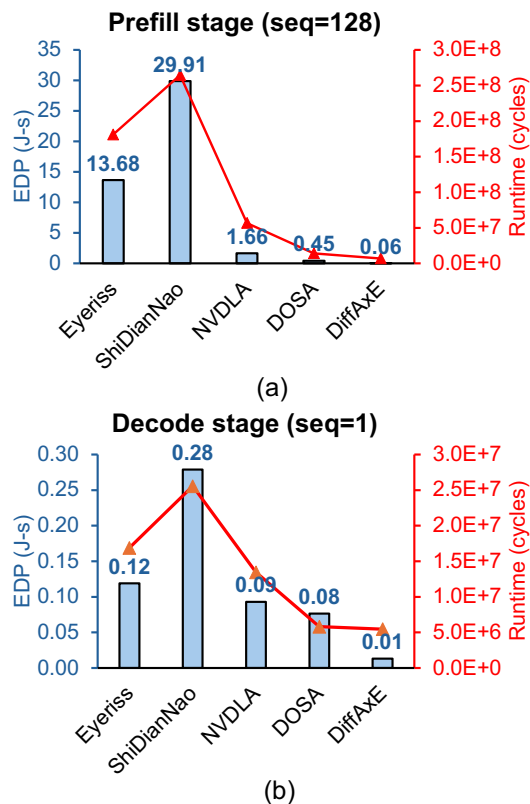


Fig. 24. EDP and runtime of different architectures for BERT-base (a) prefill and (b) decode stages on Xilinx Ultrascale+ VU13P FPGA; DiffAxE achieves the lowest EDP across three fixed accelerators—Eyeriss [4], ShiDianNao [40], NVDLA [34] and an optimization framework DOSA [8].

Fig. 24 shows the EDP of BERT-base prefill and decode stages during inference using the three fixed architectures, and two optimization based strategies—DOSA and DiffAxE. Clearly, DiffAxE achieves the lowest EDP among all the designs, with a **7.5x** and **8x** improvement over DOSA during prefill and decode stages respectively.

VII. CONCLUSION

In this work, we introduced DiffAxE, a generative framework for performance-conditioned AI accelerator design and design space exploration (DSE). DiffAxE scales to massive design spaces ($O(10^{17})$) while training on just $O(10^4)$ samples per workload, showing strong generalization. Validated across a comprehensive suite of 600 diverse DNN workloads, DiffAxE generates hardware designs within $\pm 5.45\%$ of the target performance in just 1.83 milliseconds per configuration, outperforming traditional optimization frameworks by over four orders of magnitude in search speed. We further extended our framework to structured DSE for EDP optimization using joint power-performance conditioning. Our approach yields up to 9.8% lower EDP compared to state-of-the-art methods such as VAESA [6], while achieving more than $145\times$ faster search. In the context of LLM inference, DiffAxE delivers $3.37\times$ and $15.95\times$ EDP improvement over existing optimization method DOSA [8] and the NVDLA [34] accelerator respectively on a 32nm ASIC implementation. When implemented on a Xilinx UltraScale+ VU13P FPGA, DiffAxE outperforms DOSA by generating hardware with $7.75\times$ lower EDP across different LLMs. Additionally, DiffAxE also discovers designs that outperform AIRCHITECT v2 and VAESA in both performance and search speed, despite requiring 32% fewer parameters than the former and $1312\times$ lower search time than VAESA. Overall, DiffAxE automates performance-driven hardware generation and fast design exploration, cutting deployment time and enabling software developers to create efficient accelerators without hardware expertise.

ACKNOWLEDGEMENT

This work was supported in part by CoCoSys, a JUMP2.0 center sponsored by DARPA and SRC, the National Science Foundation (CAREER Award, Grant #2312366, Grant #2318152), the DARPA Young Faculty Award and the DoE MMICC center SEA-CROGS (Award #DE-SC0023198).

REFERENCES

- [1] T. Zhao *et al.*, “Neural processing units for on-device machine learning: Opportunities and challenges,” in *Proceedings of the 60th Annual Design Automation Conference (DAC)*, 2023.
- [2] V. Sze, Y.-H. Chen, T.-J. Yang, and J. S. Emer, “Efficient processing of deep neural networks: A tutorial and survey,” *Proceedings of the IEEE*, vol. 105, no. 12, pp. 2295–2329, 2017.
- [3] B. Reagen *et al.*, “Weightless: Lossy weight encoding for deep neural network compression,” in *Proceedings of the 58th ACM/IEEE Design Automation Conference (DAC)*, 2021.
- [4] Y.-H. Chen *et al.*, “Eyeriss: An energy-efficient reconfigurable accelerator for deep convolutional neural networks,” in *IEEE International Solid-State Circuits Conference (ISSCC)*. IEEE, 2016, pp. 262–263.
- [5] Y. Shao *et al.*, “Simba: Scaling deep-learning inference with multi-chip-module-based architecture,” in *Proceedings of the 52nd Annual IEEE/ACM International Symposium on Microarchitecture*, 2019, pp. 14–27.
- [6] Q. Huang *et al.*, “Learning a continuous and reconstructible latent space for hardware accelerator design,” in *2022 IEEE International Symposium on Performance Analysis of Systems and Software (ISPASS)*. IEEE, 2022, pp. 277–287.
- [7] H. Touvron, M. Cord, M. Douze, F. Massa, A. Sablayrolles, and H. Jégou, “Training data-efficient image transformers & distillation through attention,” in *International conference on machine learning*. PMLR, 2021, pp. 10 347–10 357.

- [8] C. Hong *et al.*, “Dosa: Differentiable model-based one-loop search for dnn accelerators,” in *Proceedings of the 56th Annual IEEE/ACM International Symposium on Microarchitecture*, 2023, pp. 209–224.
- [9] H. Liu *et al.*, “Darts: Differentiable architecture search,” *arXiv preprint arXiv:1806.09055*, 2018.
- [10] B. Wu *et al.*, “Fbnet: Hardware-aware efficient convnet design via differentiable neural architecture search,” in *Proceedings of the IEEE/CVF conference on computer vision and pattern recognition*, 2019, pp. 10 734–10 742.
- [11] A. Parashar *et al.*, “Timeloop: A systematic approach to dnn accelerator evaluation,” in *2019 IEEE international symposium on performance analysis of systems and software (ISPASS)*. IEEE, 2019, pp. 304–315.
- [12] Y. N. Wu *et al.*, “Accelergy: An architecture-level energy estimation methodology for accelerator designs,” in *2019 IEEE/ACM International Conference on Computer-Aided Design (ICCAD)*. IEEE, 2019, pp. 1–8.
- [13] A. Samajdar *et al.*, “Scale-sim: Systolic cnn accelerator simulator,” *arXiv preprint arXiv:1811.02883*, 2018.
- [14] S.-C. Kao *et al.*, “Confucix: Autonomous hardware resource assignment for dnn accelerators using reinforcement learning,” in *2020 53rd Annual IEEE/ACM International Symposium on Microarchitecture (MICRO)*. IEEE, 2020, pp. 622–636.
- [15] —, “Gamma: Automating the hw mapping of dnn models on accelerators via genetic algorithm,” in *Proceedings of the 39th International Conference on Computer-Aided Design*, 2020, pp. 1–9.
- [16] —, “Digamma: Domain-aware genetic algorithm for hw-mapping co-optimization for dnn accelerators,” in *2022 Design, Automation & Test in Europe Conference & Exhibition (DATE)*. IEEE, 2022, pp. 232–237.
- [17] Y. Lin *et al.*, “Naas: Neural accelerator architecture search,” in *2021 58th ACM/IEEE Design Automation Conference (DAC)*. IEEE, 2021, pp. 1051–1056.
- [18] B. Reagen, J. M. Hernández-Lobato, R. Adolf, M. Gelbart, P. Whatmough, G.-Y. Wei, and D. Brooks, “A case for efficient accelerator design space exploration via bayesian optimization,” in *2017 IEEE/ACM International Symposium on Low Power Electronics and Design (ISLPED)*. IEEE, 2017, pp. 1–6.
- [19] C. Sakhuja *et al.*, “Polaris: Multi-fidelity design space exploration of deep learning accelerators,” *arXiv preprint arXiv:2412.15548*, 2024.
- [20] J. Seo *et al.*, “Airchitect v2: Learning the hardware accelerator design space through unified representations,” *arXiv preprint arXiv:2501.09954*, 2025.
- [21] A. Samajdar *et al.*, “Airchitect: Learning custom architecture design and mapping space,” *arXiv preprint arXiv:2108.08295*, 2021.
- [22] J. Blocklove *et al.*, “Chip-chat: Challenges and opportunities in conversational hardware design,” in *2023 ACM/IEEE 5th Workshop on Machine Learning for CAD (MLCAD)*. IEEE, 2023, pp. 1–6.
- [23] Y. Fu *et al.*, “Gpt4aigchip: Towards next-generation ai accelerator design automation via large language models,” in *2023 IEEE/ACM International Conference on Computer Aided Design (ICCAD)*. IEEE, 2023, pp. 1–9.
- [24] Z. Yan *et al.*, “On the viability of using llms for sw/hw co-design: An example in designing cim dnn accelerators,” in *2023 IEEE 36th International System-on-Chip Conference (SOCC)*. IEEE, 2023, pp. 1–6.
- [25] Z. Liang *et al.*, “Unleashing the potential of llms for quantum computing: A study in quantum architecture design,” *arXiv preprint arXiv:2307.08191*, 2023.
- [26] M. Li *et al.*, “Specllm: Exploring generation and review of vlsi design specification with large language model,” *arXiv preprint arXiv:2401.13266*, 2024.
- [27] C. Xu *et al.*, “Sns’s not a synthesizer: a deep-learning-based synthesis predictor,” in *Proceedings of the 49th Annual International Symposium on Computer Architecture*, 2022, pp. 847–859.
- [28] Y. Zhang *et al.*, “Grannite: Graph neural network inference for transferable power estimation,” in *2020 57th ACM/IEEE Design Automation Conference (DAC)*. IEEE, 2020, pp. 1–6.
- [29] M. Rakesh *et al.*, “Graspe: Accurate post-synthesis power estimation from rtl using graph representation learning,” in *2023 IEEE International Symposium on Circuits and Systems (ISCAS)*. IEEE, 2023, pp. 1–5.
- [30] S. Khan *et al.*, “Deepseq: Deep sequential circuit learning,” in *2024 Design, Automation & Test in Europe Conference & Exhibition (DATE)*. IEEE, 2024, pp. 1–2.
- [31] B. L. Miller, D. E. Goldberg *et al.*, “Genetic algorithms, tournament selection, and the effects of noise,” *Complex systems*, vol. 9, no. 3, pp. 193–212, 1995.
- [32] L. Feng *et al.*, “Gandse: Generative adversarial network-based design space exploration for neural network accelerator design,” *ACM Transactions on Design Automation of Electronic Systems*, vol. 28, no. 3, pp. 1–20, 2023.
- [33] C. Zhang, P. Li, G. Sun, Y. Guan, B. Xiao, and J. Cong, “Dnbuilder: Automatic mapping of diverse cnn models on fpga with memory and computation optimization,” in *Proceedings of the FPGA*, 2018, pp. 117–126.
- [34] G. Zhou, J. Zhou, and H. Lin, “Research on nvidia deep learning accelerator,” in *2018 12th IEEE International Conference on Anti-counterfeiting, Security, and Identification (ASID)*. IEEE, 2018, pp. 192–195.
- [35] R. Rombach *et al.*, “High-resolution image synthesis with latent diffusion models,” 2022. [Online]. Available: <https://arxiv.org/abs/2112.10752>
- [36] Z. Kong *et al.*, “Diffwave: A versatile diffusion model for audio synthesis,” in *International Conference on Learning Representations*, 2021.
- [37] J. Ho *et al.*, “Denoising diffusion probabilistic models,” in *Advances in Neural Information Processing Systems*, 2020.
- [38] P. Dhariwal *et al.*, “Diffusion models beat gans on image synthesis,” *Advances in Neural Information Processing Systems*, vol. 34, 2021.
- [39] A. Radford, J. Wu, R. Child, D. Luan, D. Amodei, and I. Sutskever, “Language models are unsupervised multitask learners,” *OpenAI Blog*, vol. 1, no. 8, 2019.
- [40] Z. Du *et al.*, “Shidiannao: Shifting vision processing closer to the sensor,” in *Proceedings of the 42nd annual international symposium on computer architecture*, 2015, pp. 92–104.
- [41] R. Balasubramonian, A. B. Kahng, N. Muralimanohar, A. Shafiee, and V. Srinivas, “Cacti 7: New tools for interconnect exploration in innovative off-chip memories,” *ACM Transactions on Architecture and Code Optimization (TACO)*, vol. 14, no. 2, pp. 1–25, 2017.
- [42] X. Peng *et al.*, “Dnn+ neurosim v2. 0: An end-to-end benchmarking framework for compute-in-memory accelerators for on-chip training,” *IEEE Transactions on Computer-Aided Design of Integrated Circuits and Systems*, vol. 40, no. 11, pp. 2306–2319, 2020.
- [43] I. Loshchilov and F. Hutter, “Decoupled weight decay regularization,” in *International Conference on Learning Representations (ICLR)*, 2019. [Online]. Available: <https://openreview.net/forum?id=Bkg6RiCqY7>
- [44] J. Deng, W. Dong, R. Socher, L.-J. Li, K. Li, and L. Fei-Fei, “Imagenet: A large-scale hierarchical image database,” in *2009 IEEE Conference on Computer Vision and Pattern Recognition*. IEEE, 2009, pp. 248–255.
- [45] T. Krishna *et al.*, “An open-source silicon testbed for the rapid evaluation of chiplet-based systems,” in *Proceedings of the IEEE International Symposium on High-Performance Computer Architecture (HPCA)*. IEEE, 2018.
- [46] Y. Heo and H. Kim, “A survey on chiplet-based computing systems,” *ACM Computing Surveys (CSUR)*, vol. 55, no. 12, pp. 1–35, 2023.
- [47] A. Jain *et al.*, “Multi-chiplet systems for accelerating transformer-based models,” in *Proceedings of the 56th Annual IEEE/ACM International Symposium on Microarchitecture (MICRO)*. IEEE, 2023.
- [48] Z. Wang, P. S. Nalla, J. Sun, A. A. Goksoy, S. K. Mandal, J.-s. Seo, V. A. Chhabria, J. Zhang, C. Chakrabarti, U. Y. Ogras *et al.*, “Hisim: Analytical performance modeling and design space exploration of 2.5 d/3d integration for ai computing,” *IEEE Transactions on Computer-Aided Design of Integrated Circuits and Systems*, 2025.
- [49] H. Touvron, T. Lavril, G. Izacard, T. Lacroix, B. Rozière, N. Goyal, E. Hambro, F. Azhar, A. Rodriguez, A. Joulin, E. Grave, and G. Lample, “Llama 2: Open foundation and fine-tuned chat models,” 2023.
- [50] S. Zhang, S. Roller, N. Goyal, M. Artetxe, M. Chen, S. Chen, C. Dewan, M. Diab, X. Li, X. V. Lin, T. Mihaylov, M. Ott, S. Shleifer, K. Shuster, D. Simig, P. S. Koura, A. Sridhar, T. Wang, and L. Zettlemoyer, “Opt: Open pre-trained transformer language models,” 2022.
- [51] J. Devlin, M.-W. Chang, K. Lee, and K. Toutanova, “Bert: Pre-training of deep bidirectional transformers for language understanding,” in *Proceedings of the 2019 Conference of the North American Chapter of the Association for Computational Linguistics (NAACL)*. Association for Computational Linguistics, 2019, pp. 4171–4186. [Online]. Available: <https://arxiv.org/abs/1810.04805>
- [52] Xilinx, *UltraScale Architecture and Product Data Sheet: Overview (DS890)*, AMD/Xilinx, 2022, 16 nm FinFET+, scalable architecture including Virtex UltraScale+ family with up to 12,288 DSP slices and 3.78M logic cells.
- [53] —, “Virtex ultrascale+ fpga product brief,” AMD/Xilinx, Tech. Rep., 2025, logic cells, DSP slice count, block RAM/UltraRAM capacity, and transceiver I/O stats for VU13P.
- [54] AMD/Xilinx, “Proven power reduction with amd ultrascale+ fpgas,” 2025, ultraScale+ architecture innovations in process, power gating, and performance-per-watt improvements.